第34卷 第4期 焊 接 学 报 Vol. 34 No. 4
2013年4月 TRANSACTIONS OF THE CHINA WELDING INSTITUTION April 2013

材料流动对连续驱动摩擦焊飞边形成的影响

姬书得[1]， 刘建光[2]， 张利国[1]， 邹爱丽[1]， 傅 莉[1]
(1. 沈阳航空航天大学 航空航天工程学院，沈阳 110136;
2. 哈尔滨工业大学 材料科学与工程学院，哈尔滨 150001)

摘 要: 在建立了45钢环形结构件连续驱动摩擦焊的二维热力耦合有限元模型的基础上，研究了焊接过程中的温度场与材料流动对飞边形成的影响规律. 结果表明，在摩擦阶段，材料主要沿轴向流动，而径向流动基本上为0; 在顶锻阶段，在大的轴向顶锻压力的挤压作用下，摩擦面边缘及其附近的材料主要沿径向向摩擦面外流动并形成飞边，且飞边的尺寸与弯曲程度随焊接时间的增加而增加. 同时，增加旋转频率以及轴向顶锻压力会导致飞边尺寸与弯曲程度的增加; 基于飞边形貌给出了45钢环节结构件连续驱动摩擦焊的合理焊接工艺参数.

关键词: 连续驱动摩擦焊; 材料流动; 飞边; 数值模拟
中图分类号: TG453 **文献标识码:** A **文章编号:** 0253-360X(2013)04-0031-04

姬书得

0 序 言

连续驱动摩擦焊(continuous drive friction welding, CDFW)是一种最典型的固相连接技术. 由于在焊接过程中不存在金属的熔化现象，因此连续驱动摩擦焊具有低应力、无常规熔焊缺陷、接头质量高等优点，可实现钢、铝、铜等同种或异种金属的连接，在阀门、钻杆、轴承、双金属气门等产品的制造中得到了越来越广泛的应用[1].

飞边是连续驱动摩擦焊接头的典型宏观形貌，它的出现对接头质量有着重要的影响. Luo等人[2]利用试验的方法研究了CDFW焊接管状结构时的飞边形成过程，指出焊接工艺过程对于飞边的大小有着重要影响. Sahin等人[3]、Meshram等人[4]、Sathiya等人[5]在研究CDFW时分析了飞边的形状与大小，但未涉及飞边的形成过程. Li等人[6]利用Abaqus对中碳钢的CDFW过程进行了二维有限元模拟，给出了焊接过程不同时刻的飞边形貌. 张全忠等人[7]建立了CDFW过程的三维热力耦合模型，在研究温度场与应力场的基础上，给出了飞边的形貌，但其并没有对飞边与材料流动之间的关系进行详细的描述. 与惯性摩擦焊、线性摩擦焊、搅拌摩擦焊等摩擦焊方法类似[8]，材料流动是影响连续驱动摩擦焊接头质量以及飞边形成等的重要因素. 目前讨论飞边与材料流动之间关系的研究者极少. 鉴于此，文中利用有限元软件Deform-2D研究了连续驱动摩擦焊焊接过程的温度场与材料流动行为，阐述了焊接工艺参数影响飞边形成的规律. 研究结果对于研究焊接机理、焊接工艺优化、飞边控制等具有重要的指导意义.

1 连续驱动摩擦焊的热力耦合模型

1.1 模型的网格划分

以材料为45钢的环形结构研究对象，且旋转侧试件与固定侧试件的尺寸完合相同，具体结构如图1所示. 考虑到研究对象的轴对称性以及轴向力的轴对称性，取环形件一个轴对称剖面作为计算模型进行轴对称分析，模型的网格划分如图2所示.

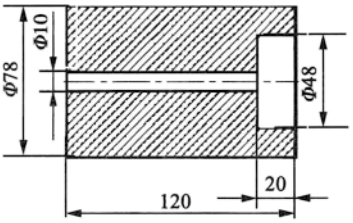

图1 连续驱动摩擦焊用环形件的尺寸(mm)
Fig. 1 Dimensions of ring structure of continuous drive friction welding

收稿日期: 2012-03-28
基金项目: 国家自然科学基金资助项目(61074090)

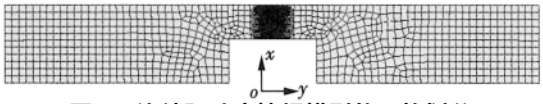

图2 连续驱动摩擦焊模型的网格划分

Fig. 2 Mesh generation of finite element model

在CDFW过程中,采用四边形单元描述试件.由于高温区域出现在摩擦界面及其附近[5],因此该区域的网格划分的比较细小以提高计算精度;远离摩擦界面的温度较低且变化幅度较小,可采用较粗大的网格进行描述.

1.2 焊接工艺参数与力学边界条件

文中的CDFW过程分成三个阶段:(1)初始摩擦阶段(0~0.2 s),在焊接过程中轴向压力是变化的,当摩擦副接触后,轴向压力逐渐增大至设定的轴向摩擦压力;(2)稳定摩擦阶段(0.2~2 s),当轴向力达到所设定的摩擦压力时,轴向压力基本保持恒定,直到摩擦结束;(3)顶锻阶段(2~4 s),轴向压力迅速升高,历时0.2 s达到设定的轴向顶锻压力时,保持不变,直到焊接过程结束.同时,在此过程中,试件的旋转频率保持不变.研究用的焊接工艺方案如表1所示.

表1 环形件连续驱动摩擦焊的焊接工艺方案

Table 1 Welding processing parameters of CDFW

工艺方案	摩擦压力 p_f/MPa	顶锻压力 p_a/MPa	旋转频率 w/(r·s^{-1})
1	20	300	20.00
2	20	200	20.00
3	20	400	20.00
4	20	300	23.33
5	20	300	26.67

在模拟过程中,固定试件的非摩擦端面上节点的自由度方向完全约束;而摩擦阶段的摩擦压力与顶锻阶段的顶锻压力作用于旋转试件的非摩擦端面上,力的方向与摩擦界面垂直.

1.3 摩擦模型的确定

在CDFW过程中,摩擦界面附近的温度经历从低温到高温的变化过程.尤其是在稳定摩擦阶段以后,摩擦界面附近的材料在高温下的屈服强度较低,那么在摩擦压力或顶锻压力的作用下剪切力将可能大于材料的剪切屈服强度.因此,文中的摩擦模型采用了经典的库仑摩擦模型和剪切摩擦模型组合而成的混合摩擦模型描述摩擦界面条件为

$$f_s = \begin{cases} -\mu p\left(\dfrac{2}{\pi}\tan^{-1}\left[\dfrac{v_s}{v_0}\right]\right) & \mu p < k \\ k & \mu p > k \end{cases} \quad (1)$$

式中:f_s为摩擦压力;μ为摩擦系数;p为焊接过程中试件间作用力;k为材料的剪切屈服强度;v_s为试件间的相对滑动速度;v_0为临界相对滑动速度.

2 CDFW过程的数值分析

2.1 焊接过程中的材料流动情况分析

由于表1提及的五个方案的温度场、材料流动、轴向缩短量、飞边等变化规律类似,下面以方案1的模拟结果进行介绍.

图3是摩擦界面的温度峰值以及旋转试件轴向缩短量随焊接时间的变化关系.通过分析可知,在CDFW过程中,摩擦面上的材料温度与试件的轴向缩短量随焊接时间的增加基本上呈现持续增加的趋势;对于温度峰值来说,在顶锻阶段初期(2~2.2 s),轴向顶锻压力迅速上升导致产热效率大幅度升高,而热量没有足够的时间向远离摩擦界面的地方传导,使摩擦面上的材料温度急剧上升;在顶锻阶段后期,尤其当材料温度超过1 100 ℃时,轴向缩短量急剧增加.这说明CDFW过程中的试件轴向缩短量主要是在焊接过程的后期产生的.

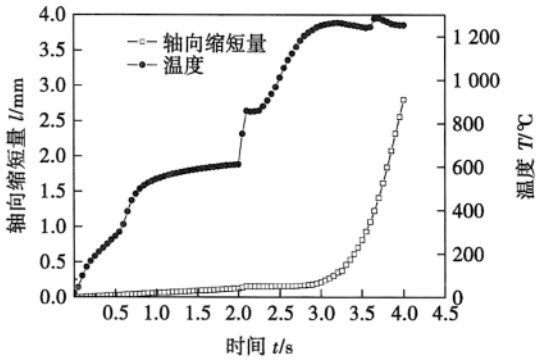

图3 摩擦面上温度峰值及试件轴向缩短量与时间的关系

Fig. 3 Change of peak value of temperature and axial shortening with welding time

图4是试件在不同时刻的材料流动速度矢量图.结合图3的结果可知,在摩擦阶段(0~2 s),试件上的温度较低使材料的流动应力较大,在较小的轴向压力作用力下,材料在径向(x方向)的流动速度基本上为0,而在轴向(y方向)上的流动速度较小,此时无飞边产生(图4a).随着顶锻过程的进行(2~4 s),由温度升高导致的材料流动应力逐渐降低,在大轴向压力作用下,材料开始在径向上流动且流动速度逐渐增加;由塑性成形理论的最小阻力定律可知,摩擦面边缘附近的金属在挤压过程中容易向摩擦面外流动而摩擦面中心处的金属流动较为困

难，因此摩擦面边缘附近的材料主要沿径向向摩擦面外流动并形成飞边且流动速度大于摩擦面中心区域的材料流动速度（图 4b ~ d）；飞边的尺寸与弯曲程度随焊接时间的增加而增加．同时，从图 4a ~ d 可知，沿轴向距摩擦面越远，材料的流动速度越小，且材料的流动方向以沿轴向流动为主．

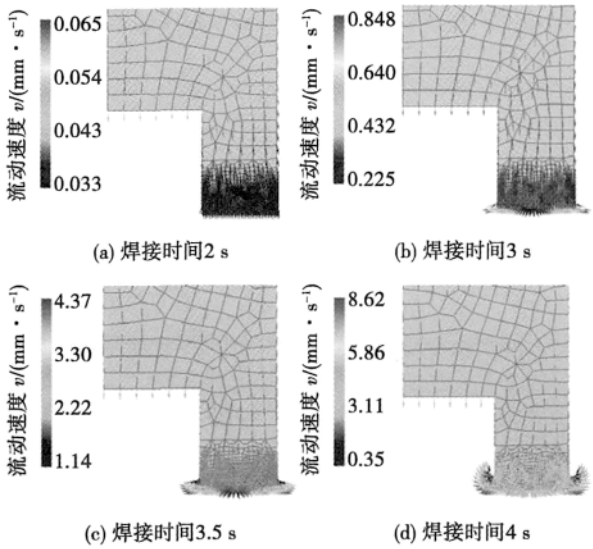

图 4　试件不同时刻的材料流动速度矢量图

Fig. 4　Flow vector of material of ring structure at different welding time

2.2　不同工艺下的温度、流动与飞边分析

图 5 是不同旋转频率下摩擦界面上温度峰值随时间的变化关系．图 6 环形件连续驱动摩擦焊的材料流动矢量与飞边形貌图．结合图 4d 可知，在顶锻阶段，随着试件转速的增加，材料摩擦面上的温度上升幅度增加，因此高旋转频率情况下摩擦面处的材料经历的高温时间长，低流动应力的材料在相同轴向压力作用下以更大的速度流动；同时，对于高旋转频率的工艺条件，在热传导的影响下，摩擦面附近的高温材料区域也会扩大，这会有利于间接提高摩擦面上材料的流动速度，对飞边的形成产生影响．因此，在其它工艺参数相同的前提下，增加试件的旋转频率会提高摩擦面上材料的流动速度及高流动速度的材料区域范围，导致试件飞边的尺寸大小以及弯曲程度的增加．

图 7 是不同顶锻压力情况下的材料流动矢量与飞边形貌图．结合图 4d 可知，在顶锻阶段，随着顶锻压力的增加，材料的流动速度增加，导致飞边的尺寸与弯曲程度增加．

在连续驱动摩擦焊过程中，飞边大小直接影响锻造程度以及界面氧化面皮等杂质的排出．当试件

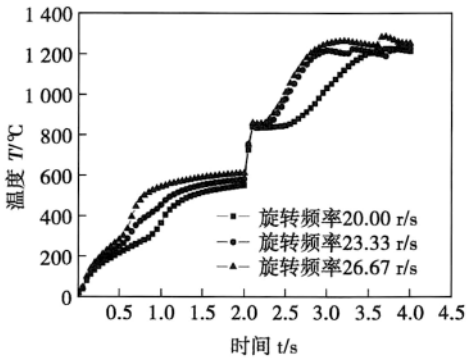

图 5　不同旋转频率下的温度峰值与时间的关系

Fig. 5　Relation between temperature peak value and welding time under different rotational velocity

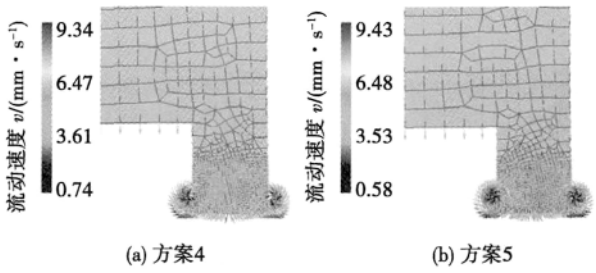

图 6　环形件连续驱动摩擦焊的材料流动速度与飞边形貌

Fig. 6　Material flow velocity and flashes shape of continuous drive friction welding of ring structure

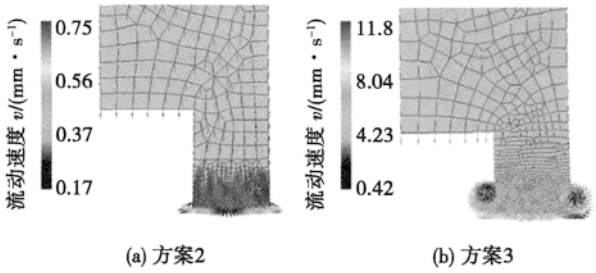

图 7　环形件连续驱动摩擦焊的材料流动速度与飞边形貌

Fig. 7　Material flow velocity and flashes shape of continuous drive friction welding of ring structure

旋转频率以及轴向顶锻压力过小时，材料的温度以及流动速度较低，导致飞边尺寸较小，此时连接区域及其附近的材料所受的顶锻作用不足，难以压实焊缝及从界面排出氧化皮等杂质．当试件旋转频率以及轴向顶锻压力过高时，材料的温度与流动速度高，导致飞边尺寸过大；此时会有过多高温材料被挤出摩擦界面，造成轴向缩短量过大甚至会使接头中心结合不良．同时，对于环状结构件来讲，飞边有外飞边与内飞边两部分，而内飞边是很难去除的．在结构件的使用过程中，内飞边上残余拉应力较高的区

域易开裂,在脱落后以颗粒的形式会对结构件的旋转中心轴产生伤害,降低其使用寿命. 综上可知,对于环形件的连续驱动摩擦焊来讲,飞边过大与过小均不好. 对于此研究对象,试件的旋转频率约为 20 r/s 且轴向压力约为 300 MPa 较好.

3 结 论

(1) 在 45 钢环形件连续驱动摩擦焊过程中,摩擦阶段的材料流动速度非常小,无飞边产生;在顶锻阶段,摩擦面边缘及其附近的材料度向面外流动并形成飞边.

(2) 增加旋转频率与顶锻压力会增加摩擦面及其附近材料向面外的流动速度,导致飞边尺寸与弯曲程度的增加;基于飞边形貌给出了 45 钢环形件连续驱动摩擦焊合理的焊接工艺参数.

参考文献:

[1] Vardhan L S, Madhusudhan R G, Mohandas T, *et al*. Continuous drive friction welding of Inconel 718 and EN24 dissimilar metal combination [J]. Materials Science and Technology, 2009, 25(7): 851 – 861.

[2] Luo J, Ye Y H, Xu J J, *et al*. A new mixed-integrated approach to control welded flashes forming process of damping-tube-gland in continuous drive friction welding [J]. Materials and Design, 2009, 30(2): 353 – 358.

[3] Sahin M, Akata H E, Gulmez T. Characterization of mechanical properties in AISI 1040 parts welded by friction welding [J]. Materials Characterization, 2007, 58(10): 1033 – 1038.

[4] Meshram S D, Mohandas T, Reddy G M. Friction welding of dissimilar pure metal [J]. Journal of Materials Processing Technology, 2007, 184(1/3): 330 – 337.

[5] Sathiya P, Aravindan S, Haq A N. Some experimental investigations on friction welded stainless steel joints [J]. Materials and Design, 2008, 29(6): 1099 – 1109.

[6] Li W Y, Wang F F. Modeling of continuous drive friction welding of mild steel [J]. Materials Science and Enginnering A, 2011, 528(18): 5921 – 5926.

[7] 张全忠, 张立文, 刘伟伟, 等. 连续驱动摩擦焊接过程的三维与二维数值模拟对比分析 [J]. 焊接学报, 2006, 27(10): 105 – 107.
Zhang Quanzhong, Zhang Liwen, Liu Weiwei, *et al*. Comparison of 3D and 2D numerical simulation of continuous-drive friction welding process [J]. Transactions of the China Welding Institute, 2006, 27(10): 105 – 107.

[8] 王非凡, 李文亚, 陈 亮, 等. 轴向压力对惯性摩擦焊的影响数值分析 [J]. 焊接学报, 2012, 33(2): 41 – 44.
Wang Feifan, Li Wenya, Chen Liang, *et al*. Numerical study on influence of axial pressure oninertia friction welding [J]. Transactions of the China Welding Institute, 2012, 33(2): 41 – 44.

作者简介: 姬书得,男,1977 年出生,博士,副教授. 主要从事摩擦焊机理、工艺与仿真方面的研究工作. 发表论文 30 余篇. Email: superjsd@163.com

[上接第 18 页]

母材的 76.82%,83.81% 和 71.20%,母材的塑性变形性能高于焊接接头的塑性变形性能.

参考文献:

[1] Geng K P, Hu S S, Shen J, *et al*. The effects of laser welding parameters on the microstructure of ferritic and duplex stainless steels welds [J]. Physics Procedia, 2010, 5: 291 – 294.

[2] Jeong K K, Yeong H K, Jong S L, *et al*. Effect of chromium content on intergranular corrosion and precipitation of Ti-stabilized ferritic stainless steels [J]. Corrosion Science, 2010, 52: 1847 – 1852.

[3] Kaul R, Ganesh P, Tripathi P, *et al*. Comparison of laser and gas tungsten arc weldments of stabilized 17% Cr ferritic stainless steel [J]. Materials and Manufacturing Processes, 2003, 18(4): 563 – 580.

[4] 丁启湛, 丁成钢, 史春元. 不锈钢的焊接 [M]. 北京: 机械工业出版社, 2009.

[5] 郑淮北, 叶晓宁, 张雪峰, 等. 12% Cr 铁素体不锈钢粗晶区组织转变和晶粒长大及析出相分析 [J]. 焊接学报, 2012, 32(6): 37 – 40.
Zheng Huaibei, Ye Xiaoning, Zhang Xuefeng, *et al*. Microstructure transformation, grain growth and precipitated phase of 12% Cr ferritic stainless steel in coarse grain zone [J]. Transactions of the China Welding Institution, 2012, 32(6): 37 – 40.

[6] 王宝森, 马朝晖, 朱双春, 等. 铁路货车用 TCS345 不锈钢焊接热影响区韧性分析 [J]. 焊接学报, 2009, 30(12): 97 – 100.
Wang Baosen, Ma Zhaohui, Zhu Shuangchun, *et al*. Analysis on heat affected zone toughness of railroad freight TCS345 stainless steel weld joints [J]. Transactions of the China Welding Institution, 2009, 30(12): 97 – 100.

[7] 王旭友, 雷 振, 毛 辉, 等. 铁素体不锈钢激光 – MAG 复合热源焊缝成形及接头冲击韧性分析 [J]. 焊接学报, 2009, 30(12): 21 – 25.
Wang Xuyou, Lei Zhen, Mao Hui, *et al*. Appearance of weld and impact toughness for the joints of ferrite stainless steel by laser-MAG hybrid welding [J]. Transactions of the China Welding Institution, 2009, 30(12): 21 – 25.

[8] 路 君, 曾小勤, 丁文江. 晶粒度与合金强度关系 [J]. 轻金属, 2008(8): 59 – 64.
Lu Jun, Zeng Xiaoqin, Ding Wenjiang. The Hall-Petch relationship [J]. Light Metals, 2008(8): 59 – 64.

[9] 钟群鹏, 赵子华. 断口学 [M]. 北京: 高等教育出版社, 2006.

作者简介: 张红霞,女,1968 年出生,博士,副教授. 主要从事材料连接及界面行为研究,焊接结构失效及安全评定等. 发表论文 20 余篇. Email: hongxzhang@163.com

welding; pulsed laser beam welding; tensile property; cupping property

Effects of keyhole-assisted gas jet on microstructure and microhardness of stainless steel laser weld SHEN Xianfeng, HUANG Wenrong, TENG Wenhua, XU Chao (Institute of Machinery Manufacturing Technology, China Academy of Engineering Physics, Mianyang 621900, China). pp 19 – 22

Abstract: Slab CO_2 continuous wave laser welding of HR-2 hydrogen-resistance stainless steel was carried out with different keyhole-assisted gas jet. During welding, the incident angle of the keyhole-assisted gas jet was 60° with a nozzle put ahead of the laser beam. The experimental results show that the layout with gas nozzle ahead of laser beam obtained better weld appearance and had little perturbation on the welding pool than that with gas nozzle behind the laser beam in gas jet-assisted keyhole laser welding. Compared with traditional laser welding, penetration depth increased significantly while penetration width decreased, and the weld shape became gourd-like with narrow middle part and wide upper and lower parts in the enhanced laser welding, because more plasma was suppressed within the keyhole and the keyhole deepened. Shorter columnar grains formed near the fusion line while equiaxed grain existed in the center of weld in enhanced laser welding, and the weld solidified by following ferrite-austenite (FA) mode. The reason for less ferrite precipitated in the weld could be resulted from the introduction of keyhole-assisted gas jet which improved the cooling condition of the weld metal.

Key words: gas jet-assisted keyhole laser welding; assisted gas jet; penetration increase; hydrogen-resistance stainless steel; microstructure

Effect of arc-ultrasonic excitation current on pores and tensile properties of MGH956 alloy TIG weld LEI Yucheng[1,2], HUANG Wei[1], XIA Xiaoping[3], ZHAO Kai[1], XIAO Bo[1] (1. School of Materials Science and Engineering, Jiangsu University, Zhenjiang 212013, China; 2. Jiangsu Province Key Laboratory of High-End Structural Materials, Jiangsu University, Zhenjiang 212013, China; 3. Tianjin Xingang Shipbuilding Heavy Industry Co., Ltd, Tianjin 300456, China). pp 23 – 26

Abstract: The arc-ultrasonic can be excited by modulating the TIG arc through high frequency. The mechanism of arc-ultrasonic was analyzed, and the effect of excitation current on pores and tensile strength of the MGH956 alloy joint made with TIG welding process was investigated. Without arc-ultrasonic, when the excitation current was 5 A and 10 A, pores in the weld obviously grew up, although the amount of pores kept almost the same. When the excitation current increased to 20 A and 30 A, the amount of pores decreased. With arc-ultrasonic, the tensile strength of the resultant joint was improved and reached the optimum value 550 MPa, 76% of that of base metal, when the excitation current was 20 A. The joints fractured with mixed brittle-ductile features.

Key words: MGH956 alloy; arc-ultrasonic; tungsten inert gas welding; pore

Mechanical properties of iron-based hard coatings prepared by plasma spraying technology LEI Ali, FENG Lajun, SHEN Wenning, WANG Guanchong (School of Materials Science and Engineering, Xi'an University of Technology, Xi'an 710048, China). pp 27 – 30

Abstract: In order to prepare wear-resistant coating on the surface of carbon steels and make the expansion coefficient of coating close to that of substrate and reduce stress in coating, mechanically mixed powders of 80% Fe, 13% P and 7% C were used to prepare iron-based wear-resistant coating by plasma spraying. The bonding strength was tested using binder dual tensile test method. The hardness in the coating was analyzed by surface microhardness method. And the wear resistance test of coating was carried out by MMW-2 (high temperature) friction and wear testing machine using 40Cr cemented carbide as grinding materials. The results show that the average bonding strength of the coating was 29 MPa, and the average microhardness was 805 HV50, higher than that of ceramic coating. The coating had better wear resistance, and the coating abrasion loss was around 36 mg which was about 1/13 of the grinding material. And the wear mechanism of the coating was mainly abrasive wear.

Key words: thermal spray; hard coating; bonding strength; microhardness; wear resistance

Effect of material flow on flash formation during continuous driven friction welding JI Shude[1], LIU Jianguang[2], ZHANG Liguo[1], ZOU Aili[1], FU Li[1] (1. Faculty of Aerospace Engineering, Shenyang Aerospace University, Shenyang 110136, China; 2. National Key Laboratory for Precision Hot Processing of Metals, Harbin Institute of Technology, Harbin 150001, China). pp 31 – 34

Abstract: The 2D coupled thermo-mechanical model was established to numerically simulate the effects of temperature and material flow on the flash formation of ring parts during continuous driven friction welding. The calculated results show that the material in friction stage mainly flew axially, while the radial velocity was nearly zero. During the forging stage, the material in or near the edge of friction surface mainly flew along the radial direction under large axial forging pressure, which resulted in the formation of flash. And the dimensions and bending degree of the flash increased with increasing of welding time, rotating speed and axial forging pressure. Based on the shape of flashes, suitable welding parameters were determined for continuous driven friction welding of 45 steel ring structures.

Key words: continuous driven friction welding; material flow; flash; numerical simulation

Recognition of spatial attitude of welding torch based on swing of rotating arc LI Xiangwen, HONG Bo, YIN Li, HONG Yuxiang (College of Mechanical Engineering, Xiangtan University, Xiangtan 411105, China). pp 35 – 37, 52

Abstract: Based on researches on scanning signal of existing arc sensors, a kind of oscillating rotating arc sensor was put forward. After analyzing the signal characteristics of the new arc sensor, the mathematical relationship between spatial attitude